J. Comput. Appl. Res. Mech. Eng. Vol. 12. No. 2, pp. 211-224, 2023 DOI: 10.22061/JCARME.2022.8081.2075

Journal of Computational and Applied Research in Mechanical Engineering

jcarme.sru.ac.ir

SRTTU

JCARM

ISSN: 2228-7922

Research paper

Thermo-elastic damping and anchor loss in the operational modes of a hemispherical shell resonator

Aylar Khooshehmehri, Abdollah Eslamimajd* and Elham Arabsheybani

Faculty of Electrical and Computer Engineering, Malek-Ashtar University of Technology, Tehran, Iran.

Article info

Article History:

Received: 16/05/2021
Revised: 22/05/2022
Accepted: 26/05/2022
Online: 29/05/2022

Keywords:
Hemispherical resonator gyroscope (HRG),
Quality factor,
Thermos-elastic damping,
Anchor loss,
Hemispherical shell resonator (HSR).

***Corresponding:**
a_eslamimajd@mut-es.ac.ir

Abstract

The hemispherical resonator gyro (HRG) is a type of precision inertial sensor that has the advantages of direct angle measurement and unlimited dynamic range. The overall accuracy of the HRG is due to the quality of its resonator shell, and improving the performance of resonators requires a proper understanding of the processes of energy damping in each resonance cycle, which has a significant impact on sensor performance. In this paper, in order to investigate the losses in the hemisphere shell resonator, first, the equations governing the shell are studied, and three-dimensional modeling is performed in COMSOL software. By performing mechanical simulations, the resonance modes and the natural frequency of the shell are investigated, and finally, the second and third resonance modes are selected as the optimal operating mode of the gyroscope. Also, by performing thermal simulations, the dominant energy damping processes, such as thermo-elastic damping and anchor loss were analyzed and simulated, and the effect of shell material on damping was investigated. Then the quality factor of the resonator was evaluated based on its geometry and material. In this way, according to the scope of work of the gyroscope, this process can be used to design the specifications of the shell to achieve a resonator with the desired quality factor.

1. Introduction

Coriolis vibration gyroscopes (CVGs) are classified into two categories: angular rate gyroscope and angular gyroscope (rate integrating gyroscope). In angular rate gyroscopes, angular velocity is measured, and to measure the angle of rotation, it is necessary to integrate the angular velocity over time. Rate integrating gyroscope directly measure the angle of rotation. They are typically made of symmetrical shells or isotropic structures such as a vibrating ring, vibrating cylinder, or vibrating hemispherical shell [1]. The idea of the CVG with a hemispherical shell resonator (HSR) was first proposed by Bryan about 130 years ago [2], and then its operational examples were used in important space and air missions, and the results were very successful and showed

low noise, long lifetime, and very high accuracy and good performance [3-6]. Due to the lightening of moving objects and flying vehicles, these gyroscopes, despite their superior performance accuracy, due to their high SWaP (size, weight, and power consumption), gave way to other types of gyroscopes, including Ring Laser Gyroscopes (RLGs) and Fiber -Optic Gyroscopes (FOGs).

With the growth of Micro Electro Mechanical Systems (MEMS) technology, the idea of implementing HRGs with this technology was introduced, and since then, various techniques for making HSRs with MEMS technology have been studied and implemented [7-9]. Among the most common of these techniques are micromachining, blowtorching, and glassblowing. Meanwhile, the glassblowing method is received more attention due to its ease of implementation, shorter sub-processes, the possibility of achieving greater symmetry, and higher quality coefficient [10-13]. Achieving HSRs in millimeter dimensions and low SWaP along with bias stability, high accuracy, and long lifetime, made HRG a strategic gyroscope in the navigation class [14].

HRGs, in addition to the resonator shell, include drive and sense electrodes and a control subsystem. In the HRG, a standing wave is formed by the drive electrodes on the shell. As the shell rotates around its axis of symmetry, the standing wave rotates under the influence of the Coriolis force. Although the rotation of the standing wave is not similar to the rotation of the shell, the difference between the rotation of the standing wave and the shell is perfectly proportional to the input rotation, and thus the input rotation would be calculated. The drive and sense electrodes can be implemented in 3D or planar structures [14]. The data that has been received from the planar electrodes is easier to process. In addition to data processing, the HSR fabrication method has been also effective in selecting the geometry of the electrodes.

Control techniques in an HRG are performed in either forced rebalance (FR) or whole angle (WA). In the FR technique, when the wave carrier shell rotates, the standing wave pattern has been controlled by electrostatic force. In this technique, the angular velocity of the wave carrier shell has been proportional to the power consumed to control the position of the standing wave and could be calculated in this way. The advantages of this control technique are high accuracy and sensitivity, but the dynamic range in this technique is limited. In the WA technique, as the wave carrier shell rotates, the standing wave pattern rotates relative to the shell. In this technique, the input rotation angle can be calculated in proportion to the rotation angle of the standing wave relative to the wave carrier shell. The advantage of this mode is that the dynamic range is large. The Northrop Grumman HRG is a gyroscope with an FR control technique, and its HSR has been covered with spherical electrodes. The HRG made by the Safran group is a gyroscope with WA control technique which its HSR has been covered with planar electrodes [15]. Although these HRGs have been designed and implemented with different types of control techniques and electrode structures, they have similar features. Extremely precise technology has been needed to make the HSR. The resonator shell symmetry is very effective on gyro functional parameters such as mechanical equilibrium, natural frequency difference, resonance deformation, and energy dissipation. In practical production, many factors, including geometric asymmetry and non-uniformity of material properties, affect the quality of the resonator shell [16]. The HSR, depending on its geometry and the shape of the anchor, is classified into types of quasi-spherical with circumferential anchor, wineglass structure with the axial anchor, and mushroom shell structure with the axial anchor. The axial anchor can also be implemented in the form of solid or hollow stems. Different shell structures have affected the shell loss factor and also lead to different quality factors and various resonance frequencies. HSRs with different structures have been implemented and studied in recent years with various fabrication techniques. The construction of a mushroom structure shell with a solid stem by the glassblowing technique has been performed in the Ref. [10], and in the Ref. [11] the design and implementation of the mushroom structure shell with a quality factor of 1 million have been described and the effect spherical symmetry of the shell is evident on the increase of quality factor. For another example

example of a mushroom structure shell, the effective mass distribution in the shell and the wet etch process on the silicon wafer before the blowing stage have been investigated in reference [17]. Adjusting the operating frequency to the appropriate range has been a feature of the resulting shell. The process of making a sample of a mushroom shell with a hollow stem using the blowtorching technique is introduced in the literature [18]. The working frequency of the resulting shell has been obtained at about 10 kHz and its quality factor has been 9.8 million, as reported in [19]. Also, in order to make a mushroom shell with a hollow stem by blowtorching method, a shell with a working frequency of 12.9 kHz and a quality factor of 271,000 has been obtained [20]. The construction and characterization of a mushroom shell with a hollow stem have been also investigated in the reference [21]. In this reference, the glass blowing method has been used to make the resonator shell. Then. In [22], the design and simulation of a hemispherical shell with a hollow stem made of polycrystalline diamond with an operating frequency of 80.61 kHz in the second resonance mode has been investigated. This shell is less sensitive to unwanted vibrations and shocks. In [23], the effect of material and geometry parameters on frequency has been examined and tries to reduce the loss and increase the quality factor in the resonator. In [24], the fused-silica resonator shell has been designed, which resonates at a natural frequency of 5.803 kHz in the second resonance mode, with a quality factor of more than 10 million. Also, the shell suitable for various space applications by examining the functional parameters of the resonator has been considered. In [25], the design of an HSR with a wineglass structure and the process of making it with the glassblowing technique have been described. In this sample, the quality factor has been increased from 6.66×10^5 to 9.32×10^5 by optimizing the blowing sub-process. Another example of a silicon oxide (SiO_2) vibrating shell has been presented in [26]. This sample is made using a pop-up-rings mask and a deep isotropic chemical etching method. Of course, spatial symmetry control in this technique requires more research. In[12], the geometric structure of the quasi-spherical resonator shell with a circumferential anchor has been studied. The quality factor of this structure has been reported as more than 2.55 million. Hemispherical resonators with an axial anchor are more sensitive and have low loss compared to the quasi-spherical structure due to the release of the resonator edge. Today, in most operational examples, mushroom structural shells with an axial stem are used.

In this paper, loss processes in the mushroom structural HSR with an axial stem are investigated. For this purpose, first, the equations governing the desired shell are studied, and three-dimensional modeling is performed in COMSOL software. By performing mechanical simulations, the resonance modes of the shell are investigated. Then, by performing thermal simulations using correction techniques in the meshing method and boundary conditions of the system, the dominant energy damping processes such as thermo-elastic damping and anchor loss were analyzed and simulated and the effect of shell material on damping was investigated. Then the quality factor of the resonator was evaluated based on its geometry and material.

In this paper, first, the mechanical simulation of the shell is presented, and the resonance modes are studied. Then, in order to investigate the quality factor of the shell, the energy loss of the system through thermal simulation is studied. In the end, a summary of the discussion is presented.

2. Mechanical simulation of HSR and determination of suitable resonance mode for gyroscopic function

To investigate the performance of the shell in different resonance modes and determine the natural frequency of the shell and its relationship with the dimensions and geometry of the HSR, it is necessary to perform mathematical modeling of the shell [20]. Fig. 1 shows the geometric parameters of the HSR. The smaller radius r, the larger radius R, the inner radius r_1, the outer radius r_2, the etched cavity depth h_e, and the shell height are given as h_s, and α is the opening angle of the shell.

According to Fig. 1 the volume of the etched cavity is calculated from Eq. (1) [27]:

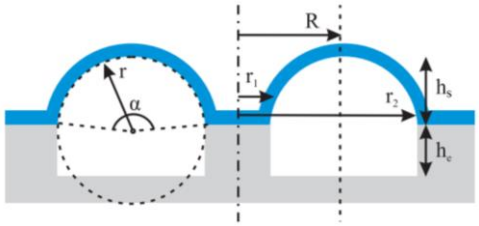

Fig. 1. Schematic of HSR with mushroom structure and axial anchor.

$$V_{cavity} = \pi(r_2^2 - r_1^2)h_e \quad (1)$$

Using geometric parameters, the shell volume can be obtained from Eq. (2) [27]:

$$V_{shell} = \pi R r^2 (\alpha - \sin(\alpha)) \quad (2)$$

According to Fig. 1 small and large radii can be obtained using Eq. (3) [27]:

$$\begin{cases} r = \dfrac{r_2 - r_1}{2\sin(\alpha/2)} \\ R = \dfrac{r_2 + r_1}{2} \end{cases} \quad (3)$$

Also, the relationship between the smaller radius (r), the opening angle of the shell (α) and the height of the shell (h_s) will be as follows:

$$h_s = r\left(1 - \cos\left(\alpha/2\right)\right) \quad (4)$$

By simulating the HSR with the mentioned characteristics, types of the resonance modes of the shell were extracted according to Fig. 2.
Fig. 2(a) shows a standing wave with a resonance mode of n = 0 on the shell. In this case, the shell has a so-called vertical or respiratory movement and this resonance mode is accompanied by contraction and expansion of the shell. In this case, no node or antinode is formed on the shell. In Fig. 2 (b), a standing wave with resonance mode n = 1 is generated on the shell. This resonance mode appears in the form of tilt and transfer movements on the shell. Gyroscopic property occurs when the standing wave has a node and antinode and is not accompanied by tilt or transfer movements, so that in addition to the possibility of sensing and measuring the rotation of the wave on the shell, it is not sensitive to external shocks and unwanted vibrations.
Therefore, the HSR will not have gyroscopic properties in n= 0, 1 resonance modes. Fig. 2 (c) shows the formation of the n =2 resonance mode. In this case, a standing wave with four nodes and four antinodes is created on the shell. Fig. 2(d) also shows a standing wave in n= 3 resonance mode with six nodes and six antinodes on the shell. Resonance modes n=2, 3 have gyroscopic properties and are resistant to environmental acceleration and shock.
Between the second and third resonance modes, the greater the angle between two consecutive nodes and the amplitude of the vibration, the greater the sensitivity. The second vibration mode n = 2 is usually used as the working mode of HRG due to these properties [28]. The frequency of the shell resonance depends on the material, geometry, and dimensions of the HSR [14], according to the simulation, the resonance frequency for mode n = 2 is 42 kHz for the HSR, whose geometric characteristics are given in Table 1.

3. Thermal simulation and extraction of HSR quality factor

In ideal vibrating systems, the energy is always constant and there is no need to supply and maintain energy in the oscillation cycle. In non-ideal vibrating systems, the vibrating energy is exposed to energy dissipating factors, such as damping through the air, friction, and the transmission of sound waves to the substrate, so it declines. Therefore, all the energy that enters the vibrating system will not be used for resonance and some of it will be converted into thermal energy. This phenomenon, in which the vibrating energy decreases due to wasting factors, is called damping. Various processes lead to energy dissipation in resonators. Some of these factors are internal and others are external.
Internal mechanisms of energy dissipation include Thermo-Elastic Damping (TED), viscoelastic damping, surface loss, and phonon-electron loss. External factors include air damping and anchor loss. Fig. 3 shows the energy dissipation processes in the shell [21].
The key to understanding energy dissipation in micro-dimension systems is to determine the mechanism of dissipation at these scales.

In micro-dimension, air damping, thermo-elastic damping, and anchor loss are usually more important than other mechanisms [29]. The quality factor of the HSR depends on the amount of energy loss of the shell and by definition, the value of the quality factor is calculated according to Eq. (1) in terms of the coefficient of partial quality factors caused by various energy loss factors:

$$\frac{1}{Q_{total}} = \frac{1}{Q_{TED}} + \frac{1}{Q_{Anchor}} + \frac{1}{Q_{Gas}} + \frac{1}{Q_{Surf}} + \frac{1}{Q_{etc}} \quad (5)$$

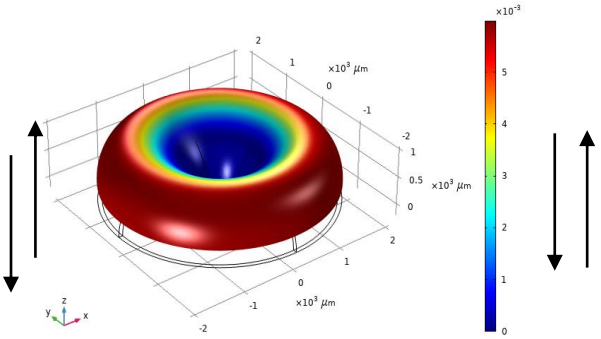

(a)

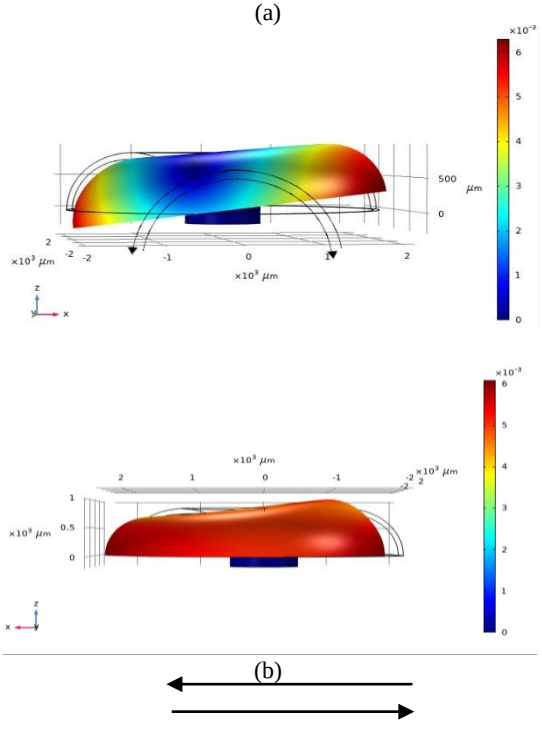

(b)

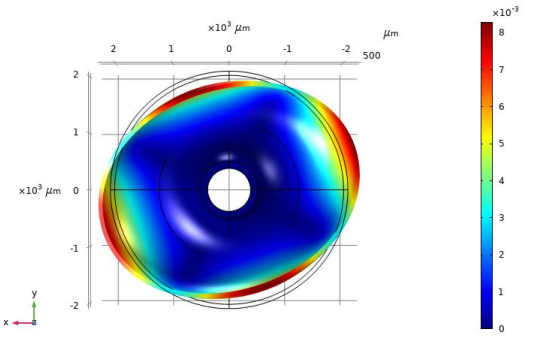

(c)

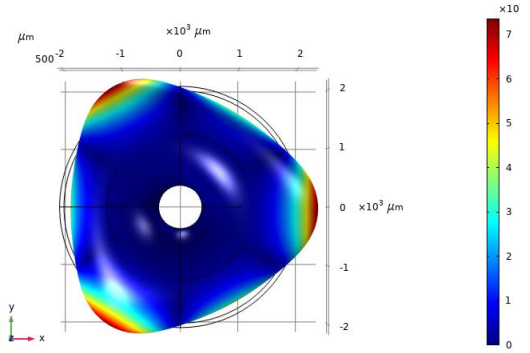

(d)

Fig. 2. Show different resonance modes of HSR with mushroom structure using COMSOL software; (a) vertical motion (n = 0), (b) tilt and transfer motion (n = 1), (c) second resonance mode (n = 2), and (d) the third resonance mode (n = 3).

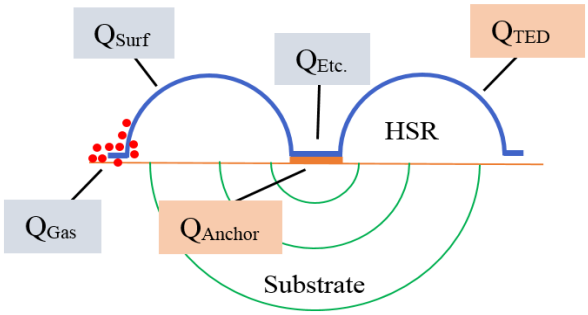

Fig. 3. Showing various energy loss factors in a HSR with a mushroom structure.

In Eq. (2), Q_{TED} is related to the thermo-elastic damping, Q_{Anchor} is related to the anchor loss, Q_{Gas} is related to the air damping, Q_{Surf} is related to the resonator surface loss, and Q_{etc} is related to other damping factors such as the internal interactions of the shell [30]. In the following, a brief explanation of each of the energy loss factors in the HSR is given.

Table 1. Geometrical and physical parameters of simulated HSR.

Parameter	Outer radius r_2	Inner radius r_1	Thickness	Density	Young's modulus	Poisson's ratio
Value	1250 µm	500 µm	100 µm	2230 kg/m^3	64 gpa	0.2

Air damping. When a moving object oscillates, the air around the moving object exerts a sticking force on the object in the opposite direction of motion, which is called adhesion loss. By placing a micro-gyroscope in a vacuum chamber, the attenuation of air adhesion can be greatly reduced surface loss. Resonator shells lose energy due to structural defects such as material impurities and surface roughness.

This process of energy dissipation is especially important in small-scale systems, as the surface-to-volume ratio increases. To reduce this loss, the roughness and defects of the shell must be reduced. For example, in making shells, high-purity materials are used that have the least defects in the lattice [13].

Thermo-elastic damping. When a thermo-elastic solid begins to move and out of equilibrium, its kinetic energy, and potential energy change and become one another, causing a loss of mechanical energy. In other words, the coupling of the strain field and the temperature field in thermo-elastic solid causes a process of energy damping, which results in the system returning to equilibrium. During resonance, part of the structure that is compressed is heated and the other part that is stretched is cooled, which causes heat flux in the system. The heat flux generated goes from the compressed part to the stretched part to create thermal equilibrium in the system. The energy used to create equilibrium is not able to be stored and increases entropy and energy loss, which is called thermo-elastic damping.

Anchor loss. The hemispherical shell resonator is fixed through the anchor to the substrate so that it can vibrate freely. Loss through the anchor is caused by the propagation of a mechanical wave from the resonator to the substrate, which is the main source of energy loss in the vibrating shell. To eliminate this loss, the anchors must be at points that are considered fixed points in the wave resonance. In this way, these points do not vibrate, and the loss is reduced. The energy damping from the anchor depends on many factors. It depends on various shell parameters such as shell material properties, thickness and radius, mass imbalance, geometric asymmetry, and viscosity of the shell, and it also depends on the different characteristics of the anchor, such as material, geometry and dimensions, shape and asymmetry of the anchor relative to the shell. It also depends on the characteristics of the substrate, such as material, shape, and finally, the type of movement, shock and speed of rotation.

As mentioned, thermo-elastic loss and anchor loss are the most effective causes of energy loss in the HSR. In this paper, the simulation and analysis of these factors on the quality factor of HSR are discussed.

3.1. Simulation and analysis of thermo-elastic damping in a HSR

For thermo-elastic damping analysis, it is assumed that the HSR system is vibrating, meaning that this elastic structure can be stretched or compressed. When the vibrating shell is stretched, its temperature gradually decreases, and compression of the structure causes an increase in temperature. During the resonance, some heat is transferred from the warmer parts of the structure to the colder parts. Because thermal transport is an irreversible process, it is associated with energy loss and attenuates the resonance of the shell. Heat loss in MEMS resonance structures is of particular importance and accounts for a large part of the energy loss process. Zener suggested Eq. (6) to calculate Q_{TED} on a simple beam resonator [23].

$$\begin{cases} Q_{TED} = \dfrac{\rho C_{SP}}{E\alpha^2 T_0} \dfrac{1+(\omega_{mech}\cdot\tau_{th})^2}{\omega_{mech}\cdot\tau_{th}} \\ \tau_{th} = \dfrac{b^2}{\pi^2 D} \\ D = \dfrac{\kappa}{\rho\cdot C_{SP}} \end{cases} \quad (6)$$

In this equation, the angular frequency ω_{mech} is equal to $2\pi f$. f is the resonance frequency of the system. ρ is the shell density, α is the

coefficient of thermal expansion, C_{SP} is the specific heat capacity, E is Young's modulus coefficient, κ is the thermal conductivity, and T_0 is the nominal mean temperature. τ_{th} represents the time constant of the resonator thermal transport, b is the thickness of the beam in the bending direction, and D is the thermal diffusivity of the beam material. According to Zener's equation, Q_{TED} is equal to the product of Q_{mat} and Q_{freq}.

$$\begin{cases} Q_{mat} = \dfrac{\rho C_{SP}}{E\alpha^2 T_0} \\ Q_{freq} = \dfrac{1+(\omega_{mech}\cdot\tau_{th})^2}{\omega_{mech}\cdot\tau_{th}} \end{cases} \quad (7)$$

As shown in Eq. (7), Q_{mat} depends only on the temperature and material of the resonator and has no dependence on resonant geometry. Q_{mat} is used to select the best material. In fact, the smaller the E and α, and the larger the C_{SP} and ρ, the more suitable the material is for the resonator and the higher the quality factor of the system. Q_{freq} is a function of $\omega_{mech}\cdot\tau_{th}$. The lowest possible value for Q_{freq} occurs when $\omega_{mech}\cdot\tau_{th}=1$ that $Q_{freq}= 2$. In fact, Q_{freq} increases or decreases with $\omega_{mech}\cdot\tau_{th}$. when $\omega_{mech}\cdot\tau_{th} = 1$ (very low excitation frequency), the deformation time of the resonator is much longer than the time required for thermal transport, mechanical movement of the shell is very slow and the resonator is in the isothermal region. Therefore, the resonator is in thermal equilibrium, so the temperature gradient at the shell surface is very low, and very little energy is lost through TED. When $\omega_{mech}\cdot\tau_{th}$? 1 (high excitation frequency), the resonator deformation time is much shorter than the time required for thermal transport, in other words, the resonator vibrates rapidly. In this case, the temperature gradient on the shell changes very quickly, and there is not enough time for thermal transport, so the thermo-elastic loss is low and the resonator is in the adiabatic regime. The area between adiabatic and isothermal is divided into two hypothetical areas, quasi-isothermal and quasi-adiabatic. The resonator shell excitation frequencies are usually located in the quasi-adiabatic area and cause a small amount of thermo-elastic loss [23]. Fig. 4 shows the Q_{TED} for a Pyrex 7740 beam resonator with three different thicknesses of 100, 200, and 300 μm. The temperature in this simulation is 293.15 Kelvin.

All three samples examined in the diagram have a similar minimum Q_{TED} of 18,400. The minimum value of Q_{TED} occurs when $\omega_{mech}\cdot\tau_{th}=1$ and Q_{freq} = 2. In this case, Q_{TED} is twice Q_{mat}, and Q_{mat} is at its minimum value equal to 9214.339. The thicker the beam, the lower the minimum amount of Qmat at the resonance frequency. Because the time constant of thermal transport increases with thickness.

As shown in Eq. (6), the thermal behavior of resonators depends on their material E, C_{SP}, ρ, υ, α and k. The effect of each of these different material properties is simulated in Q_{TED}. In each simulation, one property changes while the others are constant in their intrinsic values for the Pyrex 7740. Fig. 5 shows the normalized Q_{TED}, defined as $Q / Q_{Pyrex,}$ versus the change in material properties. As can be seen from the simulation results in Fig. 5, the value of Q_{TED} depends on some properties of the structural material. As α increases, Q_{TED} decreases significantly because α is the parameter that connects the thermal and mechanical domains. Therefore, the use of materials with low α is necessary. Fig. 5 shows that increasing k decreases Q_{TED}. This is because a lower k decreases the thermal diffusivity (D) and thus increases τ_{th}, thus increasing the Q_{TED}.

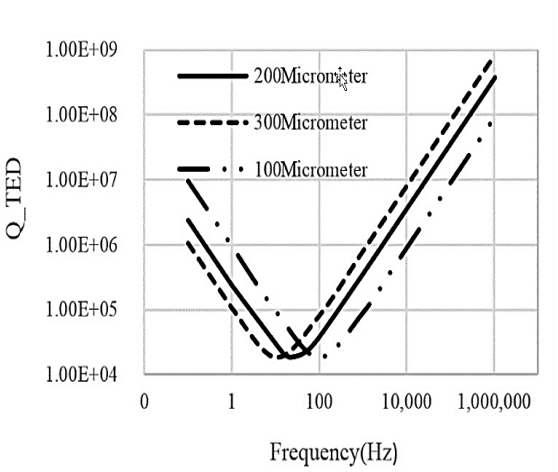

Fig. 4. Thermo-elastic dissipation curve in terms of resonance frequency.

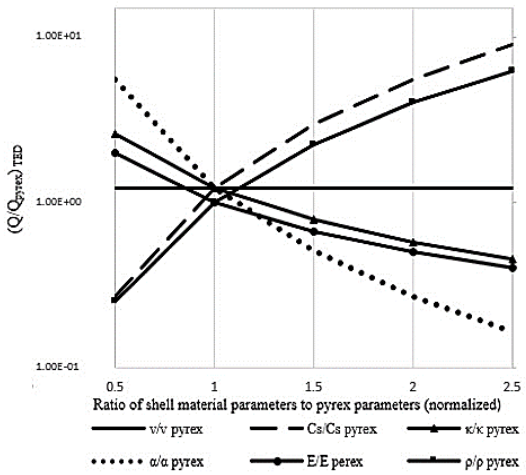

Fig. 5. Effect of shell material properties on thermo-elastic damping.

Due to the dependence of the α coefficient on Young's modulus, an increase in E increases the α and leads to a lower Q_{TED}. But the functions of E and α are not exactly the same. In fact, increasing E increases the vibration frequency of the resonator, while τ_{th} does not change.

In fact, with a further increase in E, the effects of α are expected to increase and Q_{TED} to decrease further, but unexpectedly cause the resonator to act in a more adiabatic regime, leading to higher Q_{TED}. As ρ and C_{SP} increase, the heat capacity of material $C = \rho.C_{SP}$ increases, leading to an increase in Q_{TED}.

As shown in Fig. 6, the C_{SP} parameter has a greater effect than ρ. On the other hand, increasing ρ reduces the vibration frequency and causes the shell to be less active in the area with less adiabatic properties. A change in υ changes the frequency of the vibration. According to the simulation results, Q_{TED} decreases slightly with increasing υ. The decrease in Q_{TED} is so small that Q_{TED} can be assumed to be constant. In order to investigate the relationship between Q_{TED} and shell material, six different materials have been considered for the structure of the HSR, and their Q_{TED} values have been calculated numerically, and the results of FEM simulation have been calculated, and the results can be seen in Table 3.

As can be seen in Table 3, the results of the numerical analysis are very similar to the results calculated with FEM, thus confirming the validity of the analytical model.

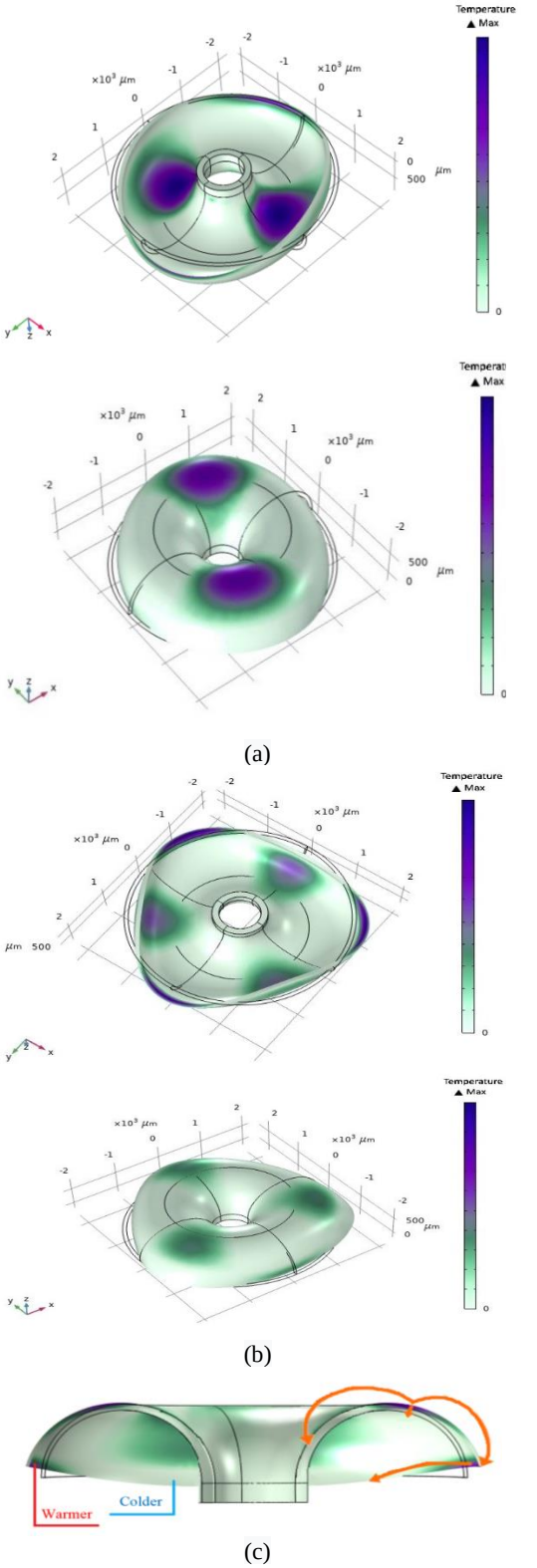

Fig. 6. thermo-elastic damping in a HSR; (a) the thermal behavior of the HSR in the second resonance mode, (b) the thermal behavior of the HSR in the third resonance mode, and (c) the path of thermal transport in the HSR.

Shells made of fused silica and silicon oxide have the highest thermo-elastic damping. This loss is due to less E, κ, and α, which leads to increase the thermo-elastic damping. These results show that the least TED is for Pyrex. Of course, thermo-elastic loss is only one of the important parameters in the selection of shell materials. Compatibility with the manufacturing process and other inherent dissipation processes are also important factors in selecting the shell material. To solve the quality factor and loss problems of HSR, the finite element numerical method is used with COMSOL software. In this simulation, other losses are ignored, and the effect of thermo-elastic loss on the quality factor is investigated. Thus, the TED factor and the total quality factor of the shell will be directly related. To explain the thermal behavior of the HSR, the simulation was performed in a three-dimensional environment of COMSOL software, and the result can be seen in Fig. 6.

By simulating the TED in COMSOL software, the thermal transport equations are solved at a temperature of 293.15 K, and the simulation result can be seen in Fig. 6. The temperature gradient on the bottom plate is constant and zero. The HSR in the second resonance mode consists of 4 nodes and 4 antinodes (Fig. 6 (a)), and the third vibrating mode consists of 6 nodes and 6 antinodes (Fig. 6(b)).

Fig. 6(c) shows the thermal transport path from the hottest to the coldest points. It is a thermal transport path at the edge of the shell that exchanges energy to the sides, up and into the shell. The other path is heat transfer in the middle structure of the shell.

Table 3 shows the values of the TED factor obtained from the COMSOL simulation in the second and third vibration modes.

According to Table 3, it is concluded that because the third resonance mode has more node and antinode points than the second resonance mode, its thermo-elastic loss is higher. Thermo-elastic loss has the opposite effect on the HSR quality factor. Therefore, the HSR quality factor based on TED in the second resonance mode is higher than the third resonance mode.

3.2. Simulation and analysis of energy loss of the HSR through the anchor

Anchor loss depends on the material, thickness and radius of HSR, mass imbalance, and geometric asymmetry of the shell. Fig. 7 shows the effects of mechanical and thermal properties of the shell on the Anchor loss. In this form, the Q normalized to Q_{pyrex} is the quality factor of the second resonance mode of the Pyrex shell. Other losses are ignored to investigate the Anchor loss factor. Thus, the quality factor and the Anchor loss factor behave exactly the same. As can be seen in Fig. 7, as Young's modulus of the shell increases, the anchor loss increases because a stiffer shell deforms the substrate more easily, leading to more energy transport (energy escape) from the shell to the substrate.

Table 2. Thermo-elastic damping in the HSR.

Resonance mode	Resonance freq. (Hz)	Q_{TED}
n=2	43.471	14.470.000
n=3	83.188	12.210.000

Table 3. Thermo-elastic damping factor for HSR with different materials.

Material	Pyrex	Fused-silica	Borosilicate	SiO_2	Silicon
E (gpa)	64	70	63	70	170
Y (1)	0.2	0.17	0.2	0.17	0.28
ρ (kg/m^3)	2200	2200	2230	2200	2329
κ (w/m.k)	1.2	1.4	1.13	¼	130
α (ppm/k)	3.25	5.0	3.3	5.0	2.6
C_{SP} (j/kg.k)	830	730	754	730	700
TED loss FEM	514.000	2.57×10^9	69.5×10^6	2.23×10^9	5.6×10^6
TED loss numerical	505.000	2.49×10^9	70.05×10^6	2.17×10^9	541.000

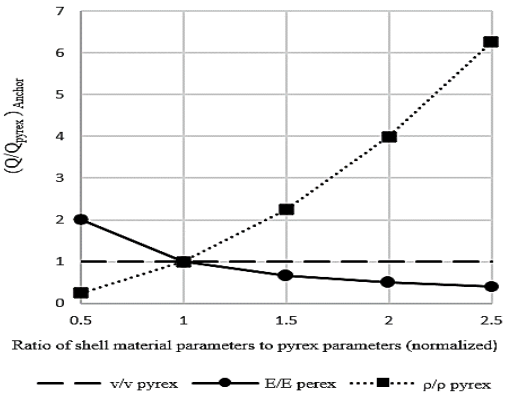

Fig. 7. Effect of shell properties on anchor loss.

Increasing the shell density also reduces the anchor loss because a denser shell conserves more kinetic energy. The effects of changing the Poisson's ratio of the shell on the anchor loss are less than Young's modulus and density, and the Poisson's ratio can be considered almost ineffective on the anchor loss [31].

To predict the mechanical energy transmitted through the anchor, the substrate of an HSR can be considered a semi-elastic material. In the anchor loss simulation, all the losses in the shell are ignored and only the energy loss through the anchor is investigated.

To investigate this, the output waves propagate over an infinite amplitude. But using the finite element method, modeling the infinite substrate is not possible. To prevent all waves from reflecting from the boundary, a non-physical absorber layer can be added along the outer boundary of the substrate to absorb all the output waves before they reach the boundary layer of the absorber layer. In the simulation process with COMSOL software, Perfectly Matched Layer (PML) can be used as an adsorbent layer. When a wave enters the PML, it attenuates exponentially and is damped by this layer. In fact, PML works as a complex material that adds damping to the waves. If the size of the PML area is large enough, the exponential collapse coefficient is guaranteed to weaken the waves.

When using PML to calculate Q, the mesh generation method is very important. In fact, poor mesh quality leads to poor convergence of COMSOL software solvers, making problem-solving difficult. In order to design the shell and substrate, the overall geometry is drawn in two-dimensional symmetrical axes in the COMSOL environment and is designed with quadrilateral mesh. Then the structure is three-dimensional with the rotation around the Z axis. The mesh quality is also selected as a very fine mesh. To minimize dissolution time, the mesh density within the PML range is variable. The mesh distribution changes from very small elements in areas close to the substrate to larger elements in areas close to the outer PML boundary. In designing the PML region, the inner radius of the region r_{PML} is also an important parameter in calculating Q. For meshing with quadrilateral elements at the cross-section, it is found that when the internal radius of the PML is small (r_{PML} <$10r_o$), the simulated quality factor fluctuates. After increasing the r_{PML} to larger values, the simulated Q becomes a fixed number. When (r_{PML}> $20r_o$), the difference between the simulated Qs is less than 10%. Therefore, the size of $r_{PML} = 20\ r_o$ is appropriate. To get an accurate result, the thickness of the PML region (the difference between the outer radius and the inner radius) depends on the wavelength emitted in each simulation. For an HSR, the wavelength is:

$$\begin{cases} \lambda = \dfrac{C}{f} \\ C = \sqrt{\dfrac{E(1-\upsilon)}{\rho(1+\upsilon)(1-2\upsilon)}} \end{cases} \tag{8}$$

In Eq. (8), λ is the wavelength propagated in the substrate, C is the speed of sound in the substrate, and f is the resonance frequency of the shell. The speed of sound in the substrate depends on the type of substrate. Also, E is Young's modulus, ρ is the density and υ is the Poisson's ratio. If a PML region with wavelength thickness is used, the waves are attenuated before reaching the PML boundary. If the PML region is shorter than the wavelength, some of the waves may not be completely attenuated and return to the resonator shell, causing the Q value to be incorrect. In addition to the PML mesh quality, internal radius and thickness, the scale coefficient α_{PML} also affects the simulation results. In fact, changing the value of α may cause inaccuracies in the calculation of Q. According to the studies, the change from 0.2 to 2 gives the same quality factor. Therefore, in this simulation, α =1 is considered, and for α outside this range, a different quality factor is obtained, which is incorrect. To simulate the

anchor loss, the shell is assumed to be Pyrex and the PML region to be silicon. Table 4 lists the parameters of the HSR and PML region.

Table 4. Parameters of HSR and PML region.

Parameter	Unit	Value
Shell radius (r_0)	µm	1750
Shell material	-	pyrex
Inner radius of PML region (r_{PML})	µm	20 r_o
Outer radius of PML region (R_{PML})	µm	λ+ r_{PML}
PML material	-	silicon
Young's modulus (E)	gpa	170
Poisson's ratio (υ)	-	0.28
Density (ρ)	kg/m^3	2329
Thermal conductivity (κ)	w/m.k	130
Specific heat (Cp)	j/kg.k	700
Thermal expansion coefficient (α)	ppm/k	2.6

Table 5. Value of anchor loss of HSR.

Resonance mode	Q_{Anchor}
n=2	62000
n=3	64200

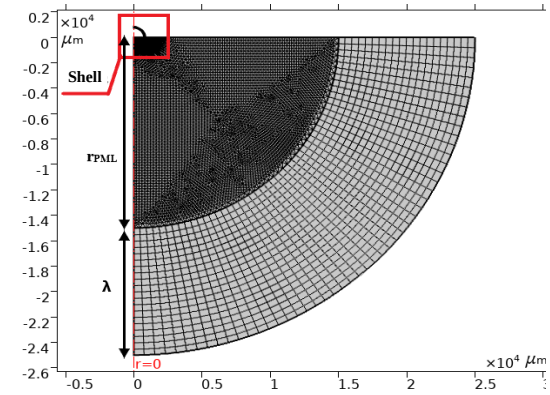

(a)

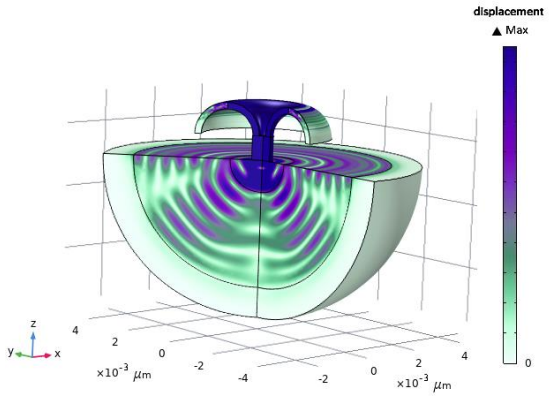

(b)

Fig. 8. Two-dimensional and three-dimensional simulation of anchor loss in COMSOL software; (a) two-dimensional design of the shell and PML region and (b) three-dimensional view of anchor loss and energy escape from the shell to the substrate.

In each resonance mode, the size of the inner and outer radii of the PML region changes according to the amount of resonance frequency. Therefore, in any resonance mode, the shell and the substrate must be redesigned. Finally, after designing in a two-dimensional symmetric axial environment in COMSOL software and applying boundary conditions, the anchor loss is obtained. Fig. 8 shows the symmetrical two-dimensional and three-dimensional design of the shell and the substrate. Thus, the amount of anchor loss factor is calculated by software and can be seen in Table 5. It shows the value of the anchor loss factor in the third resonance mode is higher than in the second resonance mode. As a result, the shell quality factor due to the amount of anchor loss in the third resonance mode is more than in the second resonance mode.

4. Conclusions

In this paper, in order to evaluate the performance and quality of the HSR, first modeling and formulation were performed, and then the mechanical resonance modes of the shell were studied. The result of the mechanical simulation is the selection of the second and third resonance modes as the working mode of the gyroscope. Then the quality factor affected by the dominant loss processes including TED and anchor loss was investigated. As a result, the quality factor of HSR based on TED in the second resonance mode is higher than in the third resonance mode. By using correction techniques in the meshing method and boundary conditions of the system in COMSOL software, HSR was simulated with FEM and PML. Due to the relationship between shell material and oscillation energy loss, the quality factor was extracted depending on the different types of shell. As a result, the shell quality factor due to the amount of anchor loss in the third resonance mode is more than in the second resonance mode. Thus, in accordance with the scope of work of the HRG, the design of the HSR with appropriate specifications can be done by studying the quality factor and resonance characteristics, including resonance mode and resonance frequency based on the geometric and mechanical parameters of the HSR.

Acknowledgment

This work is completely self-supporting, thereby no financial agency's role is available.

References

[1] A. Vafanejad, *Wineglass Mode Resonators, Their Applications and Study of Their Quality Factor*, PhD thesis, University of Southern California, (2015).

[2] B. George "On the beats in the vibrations of a revolving cylinder or bell", *Math. Proc. Cambridge Philos. Soc.*, Vol. 7, No. 24, pp. 101-111, (1890).

[3] D. M. Rozelle, "The hemispherical resonator gyro: From wineglass to the planets." *In Proc. 19th AAS/AIAA Space Flight Mechanics Meeting*, pp. 1157-1178, (2009).

[4] I. P. Prikhodko, A. A. Trusov and A. M. Shkel, "Compensation of drifts in high-Q MEMS gyroscopes using temperature self-sensing." *Sens. Actuators.*, Vol. 201, No. 3, pp. 517-524, (2013).

[5] E. C. Litty, L. L. Gresham, P. A. Toole, D. A. Beisecker , "Hemispherical resonator gyro: an IRU for Cassini." *In Cassini/Huygens: A Mission to the Saturnian Systems, International Society for Optics and Photonics*, pp. 299-310, (1996).

[6] Y. Li, L. Bing, W. Xu, and W. Wenqi, "Quadrature control of hemispherical resonator gyro based on FPGA." *10th International Conference on Electronic Measurement & Instruments, IEEE*, pp. 369-372, (2011).

[7] E. Jesper Eklund, A. M. Shkel, "Glass blowing on a wafer level", *J. Microelectromech. Syst.*, Vol. 16, No. 2, pp. 232-239, (2007).

[8] R. Lutwak, "Micro-technology for positioning, navigation, and timing towards PNT everywhere and always." *International Symposium on Inertial Sensors and Systems, IEEE*, pp. 1-4, (2014).

[9] M. H. Asadian,Y. Wang, S. Askari and A. Shkel. "Controlled capacitive gaps for electrostatic actuation and tuning of 3D fused quartz micro wineglass resonator gyroscope." *International Symposium on Inertial Sensors and Systems, IEEE*, pp. 1-4. IEEE, (2017).

[10] D. Senkal, C. R. Christopher, A. A. Trusov and A. M. Shkel, "Titania silicate/fused quartz glassblowing for 3-D fabrication of low internal loss wineglass micro-structures." *In Solid-State Sensors, Actuators, and Microsystems Workshop*, pp. 267-270, (2012).

[11] D. Senkal, M. J. Ahamed, M. H. Asadian Ardakani, S. Askari and A. M. Shkel, "Demonstration of 1 million $ q $-factor on microglassblown wineglass resonators with out-of-plane electrostatic transduction." *J. Microelectromech. Syst*, Vol. 24, No. 1, pp. 29-37, (2014).

[12] C. Jae Yoong and K. H. Najafi. "A high-q all-fused silica solid-stem wineglass hemispherical resonator formed using micro blow torching and welding." *28th IEEE International Conference on Micro Electro Mechanical Systems (MEMS)*, pp. 821-824, IEEE, (2015).

[13] D. Senkal, M. J. Ahamed, S. Askari and A. M. Shkel. "1 million Q-factor demonstrated on micro-glassblown fused silica wineglass resonators with out-of-plane electrostatic transduction." *In Hilton Head Workshop*, pp. 68-71. (2014).

[14] R. Sedaghati and M. Mahmoudian. "Hemispherical Vibratory Gyroscope Performance Evaluation and Sensitivity Analysis with Capacitive Excitation." *J. Electr. Comput. Eng. Innovations*, Vol. 7, No. 1, pp. 47-58, (2018).

[15] Z. Xu, G. Yi, H. Fang, Y. Cao, L. Hu and G. Zhang. "Influence of elasticity modulus on the natural frequency in hemispherical resonator." *DGON Inertial Sensors and Systems, IEEE*, pp. 1-11, (2019).

[16] J. Zhang, J. Shang, B. Luo and Z. Su, "Micro Fountain-Like Resonators." *IEEE 69th Electronic Components and*

Technology Conference (ECTC), pp. 890-895, (2019).

[17] T. Nagourney, S. Singh, B. Shiari, J. Y. Cho and Kh. Najafi, "Fabrication of hemispherical fused silica micro-resonator with tailored stiffness and mass distribution." *IEEE Micro Electro Mechanical Systems (MEMS)*, pp. 1000-1003, (2018).

[18] J. Y. Cho, J. Yan, J. A. Gregory, H. W. Eberhart, R. L. Peterson and Kh. Najafi, "3-dimensional blow torch-molding of fused silica microstructures." *J. Microelectromech. Syst*, Vol. 22, No. 4, pp. 1276-12846, (2013).

[19] S. Singh, T. Nagourney, J. Yoong Cho, Kh. Darvishian, and B. Shiari, "Design and fabrication of high-Q birdbath resonator for MEMS gyroscopes." *IEEE/ION Position, Location and Navigation Symposium (PLANS)*, pp. 15-19, (2018).

[20] T. Nagourney, J. Cho, A. Darvishian, B. Shiari and Kh. Najafi. "Micromachined high-Q fused silica bell resonator with complex profile curvature realized using 3D micro blowtorch molding." *18th International Conference on Solid-State Sensors, Actuators and Microsystems (TRANSDUCERS), IEEE*, pp. 1311-1314, (2015).

[21] B. Luo, J. Shang, Z. Su, J. Zhang and C. P. Wong, "Height adjustment of 3-D axisymmetric microumbrella shells for tailoring wineglass frequency." *IEEE Trans. Components, Hybrids Manuf. Technol*., Vol. 9, No. 3, pp. 567-574, (2018).

[22] Z. Liu, W. Zhang, F. Cui and J. Tang. "Three-dimensional micromachined diamond birdbath shell resonator on silicon substrate." *Microsyst. Technol*., Vol. 26, No. 4, pp. 1293-1299, (2020).

[23] A. Darvishian, T. Nagourney, J. Yoong Cho, B. Shiari and Kh. Najafi, "Thermoelastic dissipation in micromachined birdbath shell resonators." *J. Microelectromech. Syst*., Vol. 26, No. 4, pp.758-772, (2017).

[24] J. Y. Cho, S. Singh, J. K. Woo, G. He and Kh. Najafi, "0.00016 deg/√ hr Angle Random Walk (ARW) and 0.0014 deg/hr Bias Instability (BI) from a 5.2 MQ and 1-cm Precision Shell Integrating (PSI) Gyroscope." *IEEE International Symposium on Inertial Sensors and Systems (INERTIAL)*, pp. 1-4, (2020).

[25] M. J. Ahamed, D. Senkal, and A. M. Shkel, "Effect of annealing on mechanical quality factor of fused quartz hemispherical resonator." *International Symposium on Inertial Sensors and Systems (ISISS)*, pp. 1-4, (2014).

[26] M. M. Torunbalci, S. Dai, A. Bhat and S. A. Bhave, "Acceleration insensitive hemispherical shell resonators using pop-up rings." *IEEE Micro Electro Mechanical Systems (MEMS)*, pp. 956-959, (2018).

[27] D. Senkal, *Micro-glassblowing Paradigm for Realization of Rate Integrating Gyroscopes*, PhD thesis, UC Irvine, (2015).

[28] C. L. Mayberry, *Interface circuits for readout and control of a micro-hemispherical resonating gyroscope*, PhD thesis, Georgia Institute of Technology, (2014).

[29] P. Shao, *Microscale hemispherical shell resonating gyroscopes*, PhD thesis, Georgia Institute of Technology, (2014).

[30] M. Sharma, *Design and Modeling of Advanced Gyroscopes*, Master thesis, the University of British Columbia, (2006).

[31] A. Darvishian, B. Shiari, J. Y. Cho, T. Nagourney and K. Najafi, “Anchor Loss in Hemispherical Shell Resonators,” *J. Microelectromech. Syst*, Vol. 26, No. 1, pp. 51-66, (2017).

How to cite this paper:

Aylar Khooshehmehri, Abdollah Eslamimajd and Elham Arabsheybani, "Thermo-elastic damping and anchor loss in the operational modes of a hemispherical shell resonator*", J. Comput. Appl. Res. Mech. Eng.*, Vol. 12, No. 2, pp. 211-224, (2023).

DOI: 10.22061/JCARME.2022.8081.2075

URL: https://jcarme.sru.ac.ir/?_action=showPDF&article=1716